Numerical Study of In-Situ Acoustic Impedance and Reflection Coefficient Estimation of Locally Reacting Surfaces with Pressure-Velocity Probes

G. Carrillo, D. Fernández, D. Cabo, and A. Prieto

Abstract The characterization of the acoustic sound pressure and velocity field on the surface of absorbing materials plays a key role for the computation of their surface impedance and absorption coefficients. In this work, a technique based on the equivalent source method (ESM) is used to estimate the pressure and velocity field in order to compute the surface impedance and reflection coefficient of a locally reacting surface. The assessed in-situ technique only requires measuring on a single layer with an array of pressure-velocity (p-u) probes. A numerical simulation study is performed to compare the estimated values with those obtained using a double layer of pressure sensors. Results show a significant improvement in the lower frequency range in terms of both reconstruction accuracy and robustness against noise.

1 Introduction

The in-situ characterization of acoustic impedance and reflection coefficient of materials is of considerable interest for a wide range of applications. There has been an increasing amount of literature on novel in-situ methods which can be categorized in two major groups. On the one hand, several methods rely upon assumptions about the excitation sound source and the reflected sound field [1–3], such as planar, mirror model with planar reflection or spherical wave model. Such techniques often suffer from limitations when the assumptions are not satisfied in a real environment. On the other hand, sound field reconstruction techniques can also be applied without prior information about the sound field. One of the most commons methods was introduced by Tamura [4] based on the spatial Fourier

G. Carrillo (✉) · D. Fernández · D. Cabo
Microflown Technologies, Arnhem, Netherlands
e-mail: carrillo@microflown.com

A. Prieto
CITIC, Department of Mathematics, Universidade da Coruña, Coruña, Spain
e-mail: andres.prieto@udc.es

M. Cruz et al. (eds.), *Progress in Industrial Mathematics: Success Stories*,
SEMA SIMAI Springer Series 5, https://doi.org/10.1007/978-3-030-61844-5_5

Transform of sound pressure measurements at two parallel planes. With a similar configuration, an in-situ technique based on the Equivalent Source Method (ESM) was presented by Zhang et al. [5]. The ESM method has significant advantages over Tamura technique, such as a smaller measurement aperture and more accurate results. In contrast, it is currently limited to locally reactive materials because the ESM-based method is not able to account for the changes of the reflection coefficient with the angle of incidence [5]. In addition, a novel technique has recently been proposed for oblique incidence based on statistically optimized near-field acoustic holography (SONAH) also using several layers of sound pressure microphones [6].

Along with the introduction of particle velocity transducers for sound field characterization, reconstruction techniques have also been developed using a single-layer of *p-u* probes [7, 8]. Although ESM-based methods have already been used in combination with sound pressure microphones and particle velocity sensors, a comparison of the performance achieved when determining surface impedance and reflection coefficient has not yet been undertaken.

In this chapter, ESM-based methods are studied for the determination of the surface impedance and the reflection coefficient of locally reactive surfaces. Results obtained with a single layer of sound pressure microphones and particle velocity sensors (*p-u*) are compared with a double layer configuration of sound pressure microphones. In the following sections the theory of the ESM-based methods is described for both single layer and two layers case. A numerical study is presented, including results and a discussion about the performance of both methods.

2 Measurement Technique Based on Equivalent Source Method

ESM relies on modeling the sound field as the superposition of waves generated by a set of point sources. This key concept allows for splitting the contributions of different sources and it can be used for separating the incoming and reflected sound field. Accordingly, the idea is also suitable for the characterization of the surface impedance and the reflection coefficient of multiple materials.

The evaluated techniques use sound pressure or/and particle-velocity measured in one or two planes in the near-field of the tested sample, while the sound field is excited by a sound source at normal incidence. Inverse methods are applied to estimate the strength of the sound source and its image source, in such a way that the sound field on the surface can be recovered. As a result, the surface impedance and reflection coefficient can then be computed. In the following sections a general formulation of ESM for single layer of pressure-velocity probes and a double layer of pressure microphones is described. A sketch of both approaches is shown in Fig. 1.

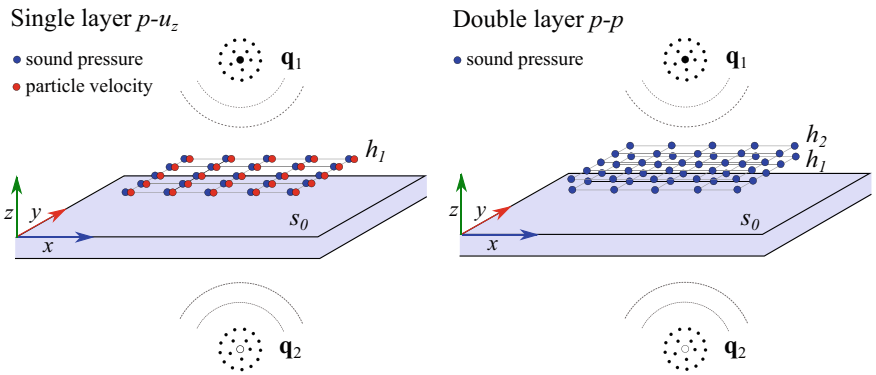

Fig. 1 Sketch of the Equivalent Source Method configuration for single layer p-u (*left*) and double layer p-p (*right*)

2.1 Theory

In the following sections the theory for the ESM is presented for both measurement configurations.

2.2 Single Layer Pressure-Velocity (p-u)

2.2.1 Forward Problem

Sound pressure and particle velocity can be expressed as the result of the superposition of the sound field created by multiple point sources. Considering the special case of having a sound source over a certain surface, the resulting sound field at the plane $z = h_1$ can be modeled as the combination of a set of equivalent sound sources $\mathbf{q}_1$ and its mirror set of image sources $\mathbf{q}_2$ as shown in Fig. 1. Hence,

$$\begin{bmatrix} \mathbf{p}_{h_1} \\ \mathbf{u}_{h_1} \end{bmatrix} = \begin{bmatrix} j\omega\rho\mathbf{G}_{q_1h_1} & j\omega\rho\mathbf{G}_{q_2h_1} \\ -\mathbf{G}^u_{q_1h_1} & -\mathbf{G}^u_{q_2h_1} \end{bmatrix} \begin{bmatrix} \mathbf{q}_1 \\ \mathbf{q}_2 \end{bmatrix}, \tag{1}$$

where the column vectors $\mathbf{p}_{h1}$ and $\mathbf{u}_{h1}$ are the pressure and the z-component of particle velocity located at the plane $z = h_1$, the vectors $\mathbf{q}_1$ and $\mathbf{q}_2$ are the equivalent source strengths that model the sound source and its image source, $\mathbf{G}_{q_ih_j}$ and $\mathbf{G}^u_{q_ih_j}$ are transfer functions that relates the propagation from the sources $\mathbf{q}_i$ to the plane $z = h_j$, ω is the angular frequency and ρ is the air density. These transfer functions are defined as the Green's function in free-space and its derivative in the normal

direction (to the measurement plane $z = h_1$), thus

$$\mathbf{G}(\mathbf{r}, \mathbf{r_0}) = \frac{e^{-jk|\mathbf{r}-\mathbf{r_0}|}}{4\pi\,|\mathbf{r}-\mathbf{r_0}|}\,, \tag{2}$$

$$\mathbf{G}^u(\mathbf{r}, \mathbf{r_0}) = \frac{\partial}{\partial z}\mathbf{G}(\mathbf{r}, \mathbf{r_0})\,, \tag{3}$$

where k is the wavenumber, $\mathbf{r}_0$ denotes the source position and $\mathbf{r}$ is the location where the sound field is computed.

2.2.2 Inverse Problem

Once the forward problem is formulated in closed form, the next step is to estimate the strength of the equivalent sources, i.e. vectors $\mathbf{q}_1$ and $\mathbf{q}_2$. Thus, an inverse problem must be solved on Eq. (1) using a weighted least squares solution as proposed in [9, 10],

$$\mathbf{q} = (\mathbf{WG})^{\dagger}\mathbf{Wb}\,, \tag{4}$$

$$\mathbf{W} = \begin{pmatrix} ||\mathbf{p}_h|| & 0 \\ 0 & ||\mathbf{u}_h|| \end{pmatrix}^{-1}\,, \tag{5}$$

where $\mathbf{q}$ is composed by the vectors of sources $\mathbf{q}_1$ and $\mathbf{q}_2$ in Eq. (1), $\mathbf{G}$ is the transfer matrix, $\mathbf{b}$ is a vector that contains the measured sound pressure $\mathbf{p}_h$ and particle velocity $\mathbf{u}_h$, and $\mathbf{W}$ is a weighting diagonal matrix. The superscript † refers to the Tikhonov regularized pseudo-inverse:

$$(\mathbf{WG})^{\dagger} = (\left[\mathbf{WG}^H\right]\mathbf{WG} + \lambda\mathbf{I})^{-1}\left[\mathbf{WG}^H\right], \tag{6}$$

where $\boldsymbol{\lambda}$ is the regularization parameter and $\mathbf{G}^H$ is the Hermitian transpose of matrix. The need of a weighting matrix $\mathbf{W}$ arises from the differences in magnitude between the sound pressure and the particle velocity by a factor which is approximately the characteristic acoustic impedance value. The application of a weighting factor avoids the residual of the minimization process to be dominated by the pressure misfit error.

2.2.3 Surface Impedance Reconstruction

The sound pressure and the particle velocity on the material surface $z = s_0$ can now be reconstructed from the estimated equivalent sources $\mathbf{q}_1$ and $\mathbf{q}_2$ and applying the

propagation Green's functions Eqs. (2) and (3). In this manner, the surface pressure and the z-component of the particle velocity are given by

$$\mathbf{p}_{s_0} = j\omega\rho(\mathbf{G}_{q_1 s_0}\mathbf{q}_1 + \mathbf{G}_{q_2 s_0}\mathbf{q}_2)\,, \tag{7}$$

$$\mathbf{u}_{s_0} = -(\mathbf{G}^u_{q_1 s_0}\mathbf{q}_1 + \mathbf{G}^u_{q_2 s_0}\mathbf{q}_2)\,. \tag{8}$$

It is possible to compute the surface impedance Z_{s_0} and reflection coefficient $R_{s_0}(\theta)$ by using the estimation of the pressure and velocity fields at N points on the surface $z = s_0$, given in Eqs. (7) and (8). Consequently, given the point values of pressure and velocity fields, $\mathbf{p}^{(n)}_{s_0}$ and $\mathbf{u}^{(n)}_{s_0}$, averaged estimates can be obtained by applying the following relationships:

$$Z_{s_0} = \frac{1}{N}\sum_{n=1}^{N}\frac{p^{(n)}_{s_0}}{u^{(n)}_{s_0}}\,, \tag{9}$$

$$R_{s_0}(\theta) = \frac{Z_{s_0}\cos\theta - Z_0}{Z_{s_0}\cos\theta + Z_0}\,, \tag{10}$$

where Z_0 is the characteristic acoustic impedance (ρc). Note that the expression of the reflection coefficient for different angles Eq. (10) is valid under the assumption of locally reactive surfaces, which holds for the present work.

2.3 Double Layer Pressure-Pressure (p-p)

As shown in [5, 11], the equivalent sources method can also be applied for sound pressure only measurements, by the use of two measurement planes $z = h_1$ and $z = h_2$,

$$\begin{bmatrix}\mathbf{p}_{h_1}\\ \mathbf{p}_{h_2}\end{bmatrix} = j\omega\rho\begin{bmatrix}\mathbf{G}_{q_1 h_1} & \mathbf{G}_{q_2 h_1}\\ \mathbf{G}_{q_1 h_2} & \mathbf{G}_{q_2 h_2}\end{bmatrix}\begin{bmatrix}\mathbf{q}_1\\ \mathbf{q}_2\end{bmatrix}\,, \tag{11}$$

where the vectors $\mathbf{p}_{h1}$ and $\mathbf{p}_{h2}$ correspond to measurements of the sound pressure on the planes $z = h_1$ and $z = h_2$; the transfer functions $\mathbf{G}_{q_i h_j}$ are given by Eq. (2) which models the sound propagation from the sources $\mathbf{q}_i$ to the plane h_j.

To solve the inversion problem, a regularized inversion approach analogous to the one presented in Sect. 2.2 is used. In this case there is no need to apply any weighting procedure. Based on the estimated equivalent source strength vectors $\mathbf{q}_1$ and $\mathbf{q}_2$, the sound pressure and the particle velocity on the surface $z = s_0$ are obtained by using Eqs. (7) and (8). The surface impedance and the reflection coefficient can then be estimated by employing Eqs. (9) and (10).

3 Numerical Study

A numerical investigation has been conducted to study the performance of the ESM-based methods described in the previous sections. Firstly, a model for the sound propagation over an impedance half-space is chosen. Next, the impedance model of a porous material is characterized. At the end, the simulation setup and the performance metric is described.

3.1 Sound Field over an Impedance Half-Space

The sound field produced by a sound source over a locally reactive surface was represented following the model proposed by Di and Gilbert [12]. The sound pressure above an infinite half-space with a given impedance is derived assuming a locally reactive surface. Thus, the sound pressure and particle velocity generated by a time-harmonic sound source of volume velocity Q at a position $\mathbf{r}$ are defined as

$$p(\mathbf{r}) = \frac{j\omega\rho Q}{4\pi}\left(\frac{e^{-jk|\mathbf{r}-\mathbf{r}_1|}}{|\mathbf{r}-\mathbf{r}_1|} + \frac{e^{-jk|\mathbf{r}-\mathbf{r}_2|}}{|\mathbf{r}-\mathbf{r}_2|} - 2k_0\beta\int_0^\infty e^{k\beta q}\frac{e^{-jk\sqrt{d_1^2+(r_{1z}+r_z-jq)^2}}}{\sqrt{d_1^2+(r_{1z}+r_z-jq)^2}}dq\right), \tag{12a}$$

$$u_z(\mathbf{r}) = \frac{-1}{j\omega\rho}\frac{\partial}{\partial z}p(\mathbf{r}), \tag{12b}$$

where $\mathbf{r}_1$ and $\mathbf{r}_2$ are the locations of the sound source and its image source, r_z and r_{1z} are the heights of the measurement point and the sound source with respect to the material surface, d_1 is the horizontal distance between the sound source and $\mathbf{r}$, and $\beta = Z_0/Z_{s_0}$ is the normalized surface acoustic admittance at normal incidence.

3.2 Locally Reacting Surface and Porous Impedance Model

The absorbing surface material under test is supposed to be locally reacting. Thus, the input impedance related to the acoustic behavior of a porous layer is assumed independent of the angle of incidence of the sound waves. Under this assumption, the ESM method could be applied and the reflection coefficient could also be computed for several angles of incidence. Without loss of generality, the model for the porous material is assumed to be of the type Delany and Bazley [13]. The surface impedance with a given flow resistivity σ (N m s^{-4}) at a frequency f is given by

$$Z_s(f) = Z_0\left[1 + 9.08(10^3 f/\sigma)^{-0.75} - j11.9(10^3 f/\sigma)^{-0.73}\right]. \tag{13}$$

3.3 Simulation Setup and Error Estimation

A sound source was placed 0.1 m above the material while a uniform line array was located at certain distance above the surface along the x-axis. For the single layer p-u configuration the array was located at $z = 0.01$ m, while the double layer p-p sensor array was at $z = 0.01$ m] and $z = 0.03$ m. The sound field was measured at 21 equally spaced points in the interval $[-0.1, 0.1]$ at the x-axis. Despite the axial symmetry of the problem, sensors were placed at both sides of the x-axis in order to account for uncorrelated noise between transducers. The equivalent sources were located in two circles with a radius of 0.01 m around the sound source and its image source, consisting of 12 elements at each location. A sketch of the problem addressed is illustrated in Fig. 2.

The noise added to the simulated data was assumed white isotropic Gaussian noise of equal variance for all transducers with a fixed signal-to-noise ratio (SNR) of 30 dB. The SNR is defined as the signal power to noise ratio: $10 \log_{10}(P_{signal}/P_{noise})$. All results presented were obtained using a Monte Carlo simulation over 100 runs.

Results are assessed by evaluating the reconstruction error with respect to the reference values. The relative error $E\{\gamma_{\text{ref}}\}$ of an arbitrary estimation γ_{est} is calculated with respect to the reference γ_{ref} as follows,

$$E\{\gamma_{\text{ref}}\} = 20 \log_{10} \left(\frac{\|\gamma_{\text{est}} - \gamma_{\text{ref}}\|_2}{\|\gamma_{\text{ref}}\|_2} \right) \tag{14}$$

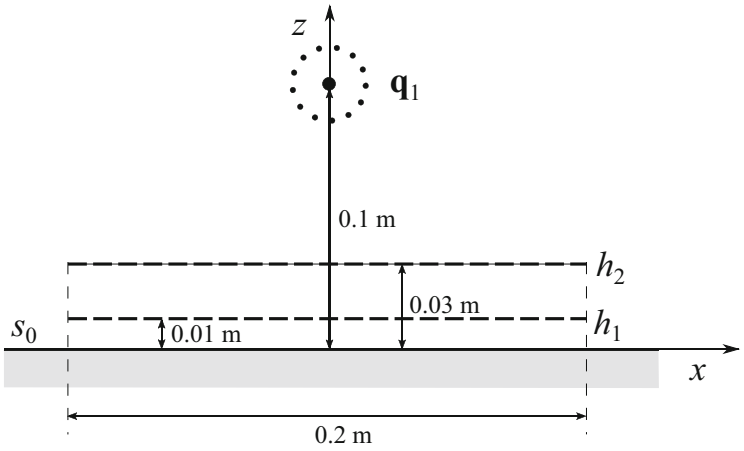

Fig. 2 Sketch of the numerical simulation configuration

4 Results and Discussion

In the following sections a numerical investigation has been performed with two main objectives:

1. To study the performance of ESM-based methods with two different configurations: single layer *p-u* and double layer *p-p* methods.
2. To assess the impact of different SNR conditions on the reconstruction error across frequency.

4.1 Surface Impedance and Reflection Coefficient

Results of normalized surface impedance estimations are shown in Fig. 3. The reconstruction error indicates that the double layer *p-p* configuration achieves a good

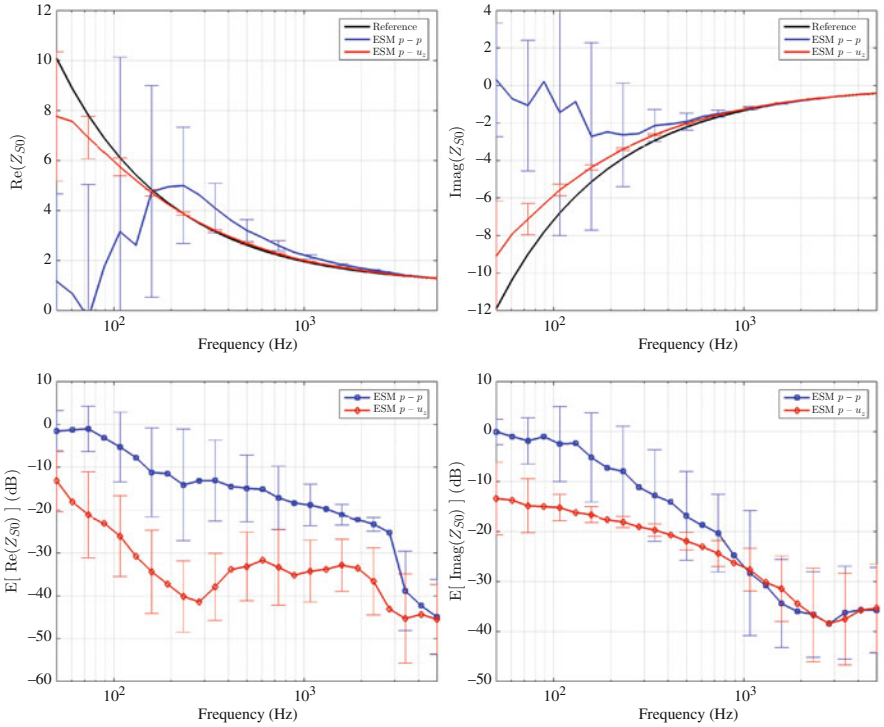

Fig. 3 Normalized complex surface impedance: real part (*top left*), imaginary part (*top right*), relative error of real part estimation (*bottom left*) and relative error of the imaginary part estimation (*bottom right*). A confident interval of 95% is displayed with the same colors as the corresponding method

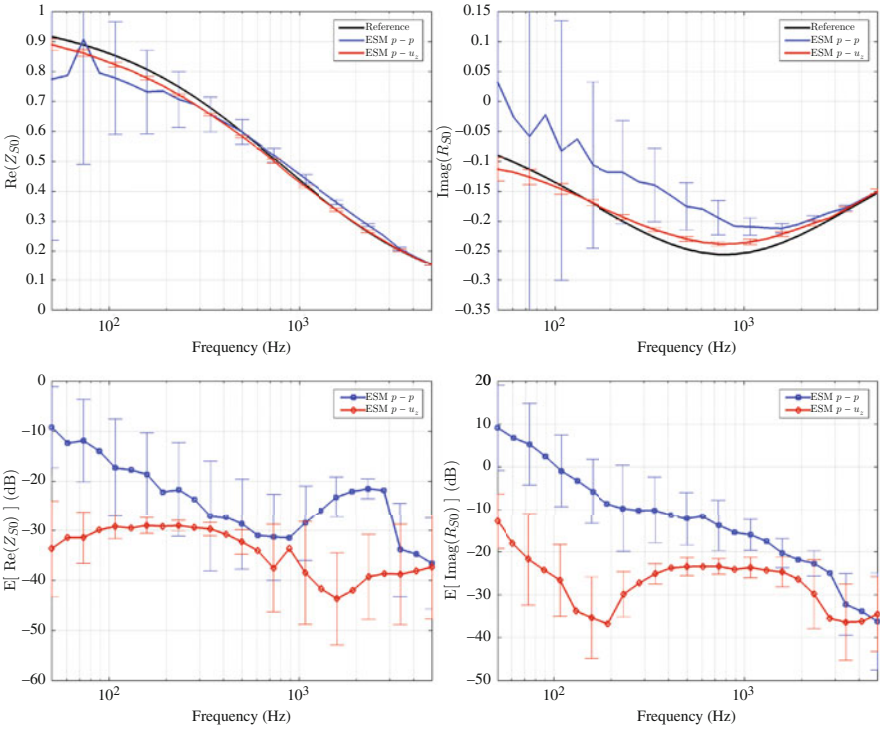

Fig. 4 Normalized complex reflection coefficient: real part (*top left*), imaginary part (*top right*), relative error of real part estimation (*bottom left*) and relative error of the imaginary part estimation (*bottom right*). A confident interval of 95% is displayed with the same colors as the corresponding method

performance for frequencies above 800–1000 Hz, where the relative reconstruction error is below −20 dB (i.e. 10% error). In contrast, the *p-u* single layer shows a good performance also for lower frequencies, even at 300 Hz.

Results obtained for the reflection coefficient R_{s_0} are presented in Fig. 4. As shown, the *p-p* double layer configuration has significant performance differences in the reconstruction of the real and the imaginary part. The reconstruction error of the imaginary part is acceptable above 1500 Hz, while the real part is valid from 200 Hz. On the other hand, the single layer *p-u* array yields accurate results from 50 Hz for both real and imaginary part of the reflection coefficient.

Interestingly, reconstruction results of the reflection coefficient using the *p-u* configuration are more consistent and less sensitive to noise than the ones obtained for the surface impedance. Furthermore, results achieved with the *p-p* configuration have a greater variance across the Monte Carlo runs. In conclusion, the reconstruction error and the variance of the results suggest that the single layer *p-u* configuration is generally more robust and accurate than the double layer *p-p* array, especially in the low frequency range.

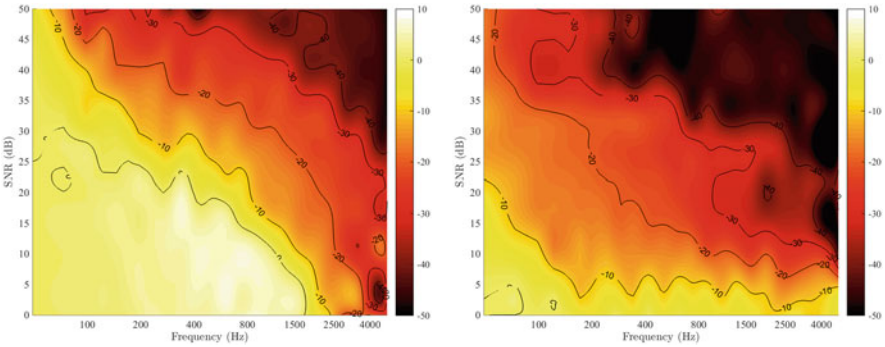

Fig. 5 Reconstruction error of the surface impedance for variable SNR and frequencies with two different sensor configurations: single layer p-u (*left*) and double layer p-p (*right*)

4.2 Surface Impedance Reconstruction Error for Variable SNR

The SNR plays a key role in the performance and robustness of ESM methods. Previous results suggest that both tested configurations are affected by noise in a different manner. In order to gain a better understanding about the influence of noise on the reconstructions, an additional Monte Carlo simulation has been undertaken. Relative reconstruction errors obtained with both configurations are presented in Fig. 5 for different levels of SNR, where brighter colors to indicate large errors.

As shown in Fig. 5, the *p-u* method significantly outperforms the *p-p* configuration, especially in the low frequency range (<1000 Hz).

4.3 Discussion and Future Research

The *p-u* method seems to outperform the alternate *p-p* method for large wavelengths (low frequency). A possible explanation for this effect could be the differences capturing the information on both methods that grant incident and mirror sound field reconstruction. As *p-p* method relies on the differences between two measurements planes, at large wavelengths, the interference patterns and the noise dominate over the differences in the sound field. The ability to acquire the two quantities at the same plane seems to be key for avoiding large estimation errors when the wavelength is large.

Nevertheless both methods seem to present a bias at very low frequency. To certain extent, it looks like that the location of the equivalent sources present difficulties to represent the scattered sound field. A future extension of this work could include the addition of equivalent sources along the impedance half-space to better capture the scattered sound field.

In addition, future research should examine the use of more elaborated impedance porous models and determine until which extend the locally reaction assumption is hold.

5 Conclusion

The acoustic properties of a locally reactive surface have been calculated using both a single-layer of *p-u* probes and a double layer of sound pressure microphones in combination with ESM. A numerical comparison of these configurations has been conducted assessing the impact of SNR on the results at different frequencies. It has been shown that both configurations yield good results (reconstruction error lower than 10%) at high frequencies, above 800 Hz for the surface impedance and 1500 Hz for the reflection coefficient. However, single layer *p-u* has a significantly better performance in the low frequency range, for wavelengths that are much larger than the distance to the surface or spacing between layers of the *p-p* configuration. In addition, the single layer *p-u* is also most robust against noise, achieving accurate results with relatively low levels of SNR.

References

1. Brandão, E., Lenzi, A., Paul, S.: Acta Acustica United Acustica **101**(3), 443 (2015)
2. Alvarez, B., Jacobsen, F.: INTER-NOISE and NOISE-CON Congress and Conference Proceedings, vol. 5, pp. 4055–4065. Institute of Noise Control Engineering (2008)
3. Nocke, C., Mellert, V., Waters-Fuller, T. Attenborough, K., Li, K.: Acta Acustica United Acustica **83**(6), 1085 (1997)
4. Tamura, M.: J. Acoust. Soc. Am. **88**(5), 2259 (1990)
5. Zhang, Y.B., Lin, W.L., Bi, C.X.: INTER-NOISE and NOISE-CON Congress and Conference Proceedings, vol. 249, pp. 3220–3227. Institute of Noise Control Engineering (2014)
6. Ottink, M., Brunskog, J., Jeong, C.H., Fernandez-Grande, E., Trojgaard, P., Tiana-Roig, E.: J. Acoust. Soc. Am. **139**(1), 41 (2016)
7. Jacobsen, F., Jaud, V.: J. Acoust. Soc. Am. **121**(3), 1550 (2007)
8. Fernandez Grande, E.: Near-field acoustic holography with sound pressure and particle velocity measurements. Ph.D. thesis, Acoustic Technology, Technical University of Denmark, Kgs. Lyngby (2012)
9. Hansen, P.C.: SIAM Rev. **34**(4), 561 (1992)
10. Fernandez-Grande, E., Jacobsen, F., Leclere, Q.: J. Acoust. Soc. Am. **132**(6), 3818 (2012)
11. Zhang, Y.B., Jacobsen, F., Bi, C.X., Chen, X.Z.: J. Acoust. Soc. Am. **126**(3), 1257 (2009)
12. Di, X., Gilbert, K.E.: J. Acoust. Soc. Am. **93**(2), 714 (1993)
13. Delany, M., Bazley, E.: Appl. Acoust. **3**(2), 105 (1970)